

Chapter 2

Relevant Background

2.1 Brief Tour of the Sun

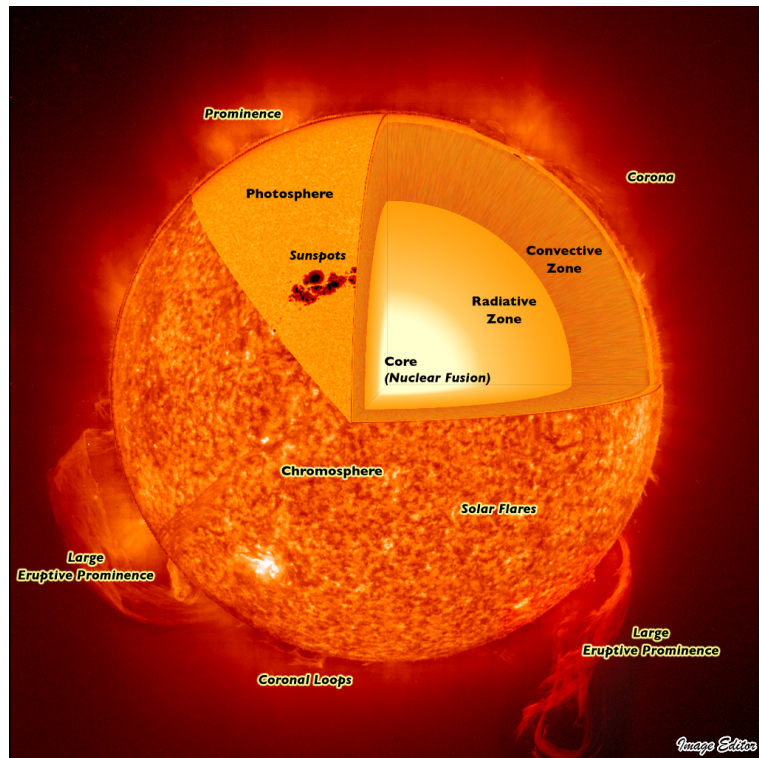


Figure 2.1: Sectional cutaway diagram of the sun to show basic structure. Figure courtesy of Image Editor on flickr.

Figure 2.1 shows the basic structure of the sun. Nuclear fusion occurs in the core and produces high-energy photons that slowly travel outward through the radiative zone. In every spherical surface centered on the core, the net energy flux outward must be positive or there

would be a steady build up of energy that would eventually cause the sun to explode. In the convection zone, the dominant form of heat transport becomes mass plasma motion that circulates hot matter upward where it cools and sinks back down. At the photosphere, the opacity drops rapidly and photons are free to fly. The undulating chromosphere lies just above the photosphere; it is vastly out-shined by the photosphere except in a few special wavelengths corresponding to dark absorption lines in the photosphere. The transition region is so named for the dramatic and unintuitive temperature increase from the chromosphere to the corona. Through the interior of the sun, the temperature and density steadily drop (see Figure 2.2) as one would expect from everyday experience: for example, you warm your hands by drawing closer to a campfire. Nevertheless, the transition region escalates the temperature, bringing the corona to ~ 1 MK. Where the sun below and far above the corona are dominated by gas dynamics, the corona itself is dominated by magnetic fields. This ratio is the definition of the β parameter:

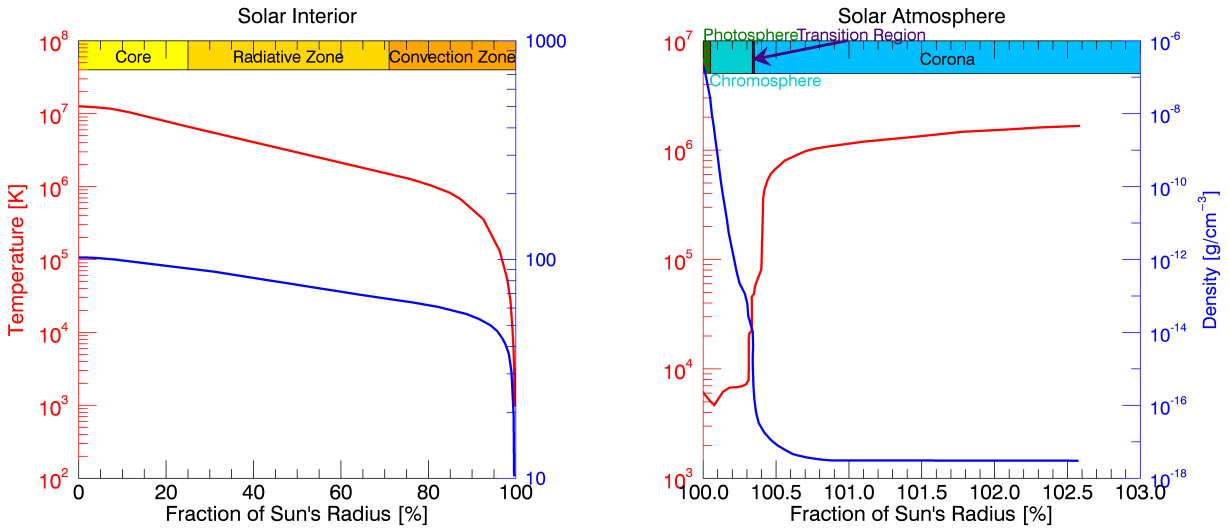


Figure 2.2: Solar temperature and density versus height from the core to the corona. Data adapted from various sources. Atmospheric temperature and density from Eddy (1979), interior temperature from Lang (2001), and interior density from Christensen-Dalsgaard et al. (1996).

$$\beta = \frac{p_{gas}}{p_{mag}} = \frac{nk_B T}{B^2/(2\mu_0)} \quad (2.1)$$

where p_{gas} is the pressure of a gas (or plasma in this case), p_{mag} is the magnetic pressure, n is the number density, k_B is Boltzmann's constant, T is temperature, B is the strength of the magnetic field, and μ_0 is the permeability of free space. When $\beta > 1$, normal gas pressure dominates and when $\beta < 1$, magnetic pressure dominates. The transition from $\beta > 1$ to $\beta < 1$ is an important one for understanding how vast amounts of energy can be stored in the solar atmosphere, providing the necessary power to drive solar eruptive events. β as a function of height above the photosphere is shown in Figure 2.3.

The following sections will step through each layer of the sun with descriptive detail proportional to their relevance to the work to be presented in later chapters.

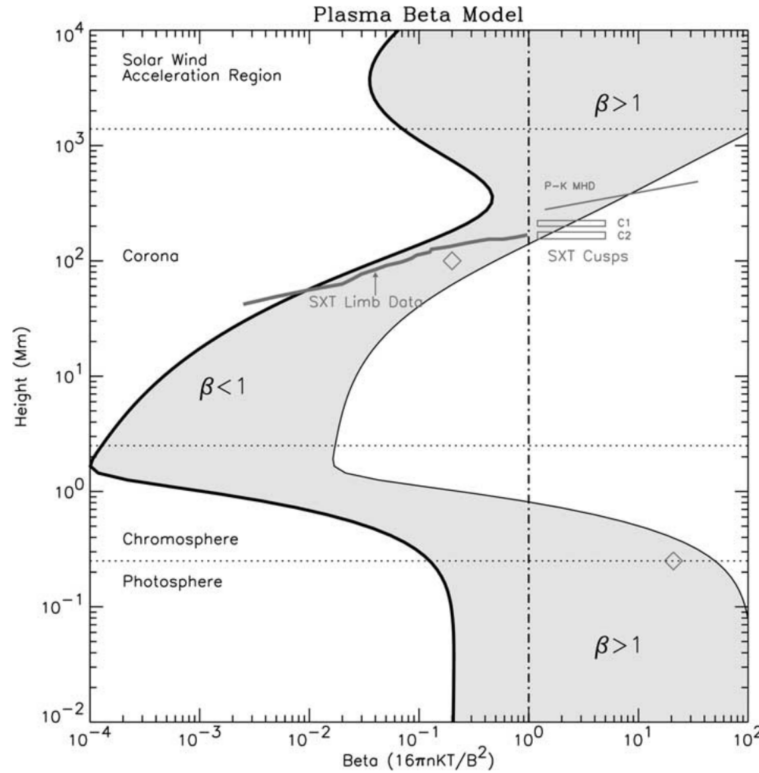


Figure 2.3: Solar plasma β versus height from the photosphere through the corona. Figure courtesy of Gary (2001).

2.1.1 Core

The gravitational pressure and density in the core of stars is sufficient to ignite nuclear fusion. In a main sequence star at the midpoint of its life, like the sun, the primary fusion reaction is the conversion of hydrogen to helium. The majority of the sun is made of hydrogen (see Figure 2.4) – a reflection of its relative abundance in the universe at large. Fusion in the core of stars is responsible for producing elements up to iron; the fusion process for elements heavier than iron is endothermic and thus cannot be used by the star to support itself against gravity. Instead, heavier elements are produced during supernovae. Supernovae also spread the source star's fusion products far away where they are incorporated into newly forming stars. Thus, the sun has observable metals¹ such as Fe even though it has not reached the point in its life where it produces them itself. The metals in these second and third generation stars are not confined to the core; rather, they can be found even in the corona. In subsequent sections it will become clear that having various elemental species at different stages of ionization in the directly observable solar atmosphere provides a means of determining temperature and structure.

2.1.2 Radiative Zone

Every nuclear reaction in the core generates high-energy photons. It takes thousands to hundreds of thousands of years for these photons to reach the photosphere because the incredible density of the solar interior results in a mean free path for photons on the order of centimeters. Because the density decreases with radial distance from the center (blue line in Figure 2.2), there is a subtle bias in the mean free path of the photons that causes the net direction to be outward. This is the physical process that characterizes the radiative zone. Additionally, temperature decreases with distance from the center (red line in Figure 2.2). When in thermodynamic equilibrium, as the solar interior is, atomic emission of photons obeys Planck's law, which describes blackbody

¹ “metals” here is in the astrophysical sense of all elements heavier than helium

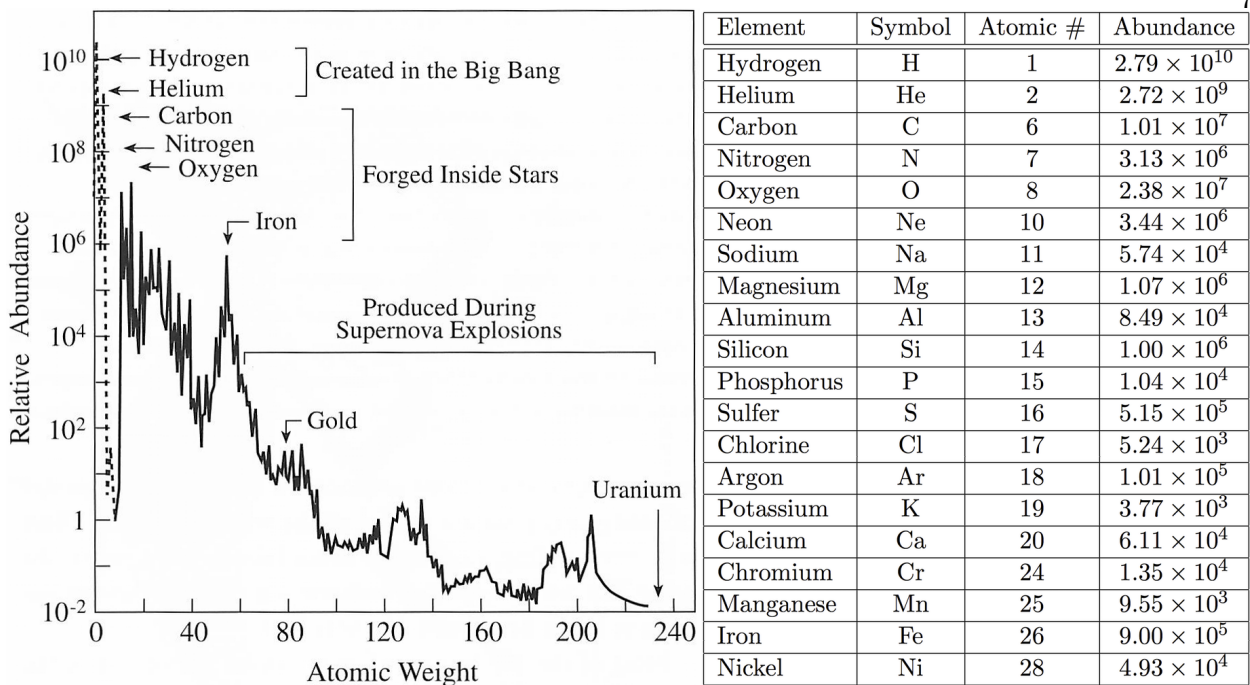


Figure 2.4: (Left) A plot of the abundance of all elements in the sun. (Right) A corresponding table of the 20 most abundant elements. Values in the plot and table are normalized to the abundance of Si, 1.00×10^6 . Figure and plot are adapted from Lang (2001).

emission:

$$S_\lambda = \frac{8\pi hc}{\lambda^5} \frac{1}{e^{hc/\lambda k_B T} - 1} \quad (2.2)$$

where S is the spectral radiance of a body at a particular temperature, λ is wavelength, h is Planck's constant, c is the speed of light, and other terms are as previously defined. This equation can be interpreted simply as a lower temperature resulting in lower energy emission (i.e., longer wavelength). Thus, as photons move outward from the core, they are absorbed by atoms at lower temperature and reemitted at longer wavelengths. In order to conserve energy, multiple photons of lower energy must be emitted. All sunlight is essentially an attenuation of the light generated in the fusing core.

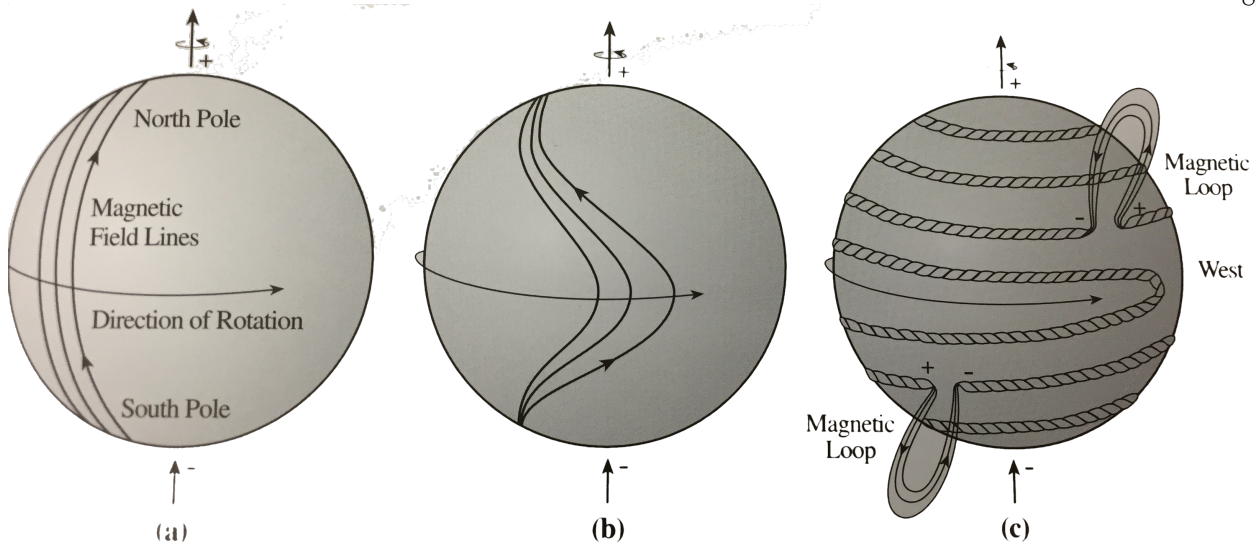


Figure 2.5: (Left) Once the solar dynamo generates a magnetic field vertically around the sun, (middle) differential rotation of the sun causes the field to wrap around the sun, (right) and any small kinks in the field are lifted by their buoyancy in an Ω loop. Figure courtesy of Lang (2001).

2.1.3 Convection Zone

At approximately 70% of the sun's radius, the dominant outward heat transport mechanism changes from radiation to convection. Plasma stores heat near the base of the zone and its buoyancy causes it to rise to a point where its heat can be rapidly dissipated (this point is the photosphere where radiative cooling becomes highly effective). The cooled plasma then sinks back down where it will again be heated at the base of the convection zone, establishing the cycle of outward heat transport. The observed convective cells at the photosphere are known as granules and supergranules. The difference between them is size and that supergranules have much slower horizontal plasma flow. Additionally, the convection zone is responsible for many of the dynamics observed in the corona (to be described in subsequent sections), which are due to the strong magnetic field and $\beta < 1$ in the corona. The magnetic field is thought to be generated at the base of the convection zone. The precise mechanism of the solar dynamo is not yet well understood, but the surfacing of the field is likely described by slight kinks in the field being lifted by plasma buoyancy (see Figure 2.5). β is large in the convection zone, so the magnetic field generated at the base is subject to

the upward plasma motion just described. Once it reaches the solar atmosphere, the magnetic field dominates and so is not pulled back down with the sinking plasma.

2.1.4 Photosphere

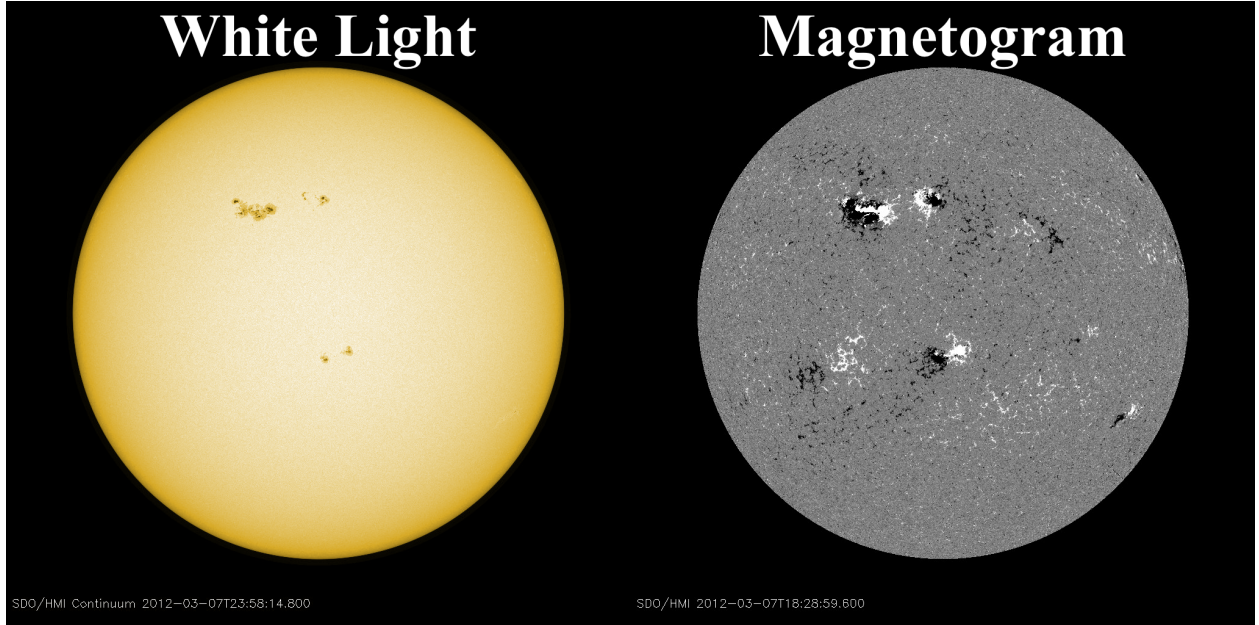


Figure 2.6: (Left) White light image of the solar photosphere on 2012 March 5. (Right) The corresponding photospheric line-of-sight magnetic field. Black indicates field into the page and white indicates field out of the page. These data come from the Helioseismic Magnetic Imager onboard the Solar Dynamics Observatory spacecraft.

The photosphere is a thin (~ 300 km or $0.05\% R_{\odot}$) layer where the opacity suddenly drops (i.e., the optical depth is unity) and photons can escape to space more or less unscathed. It is often referred to as the “surface” of the sun but this label can be misleading since the density at the photosphere is ~ 2500 times more rarefied than the *air* on top Mount Everest. The photosphere is constantly roiling; the lifetime of a granule is only about 8 minutes while supergranules last about 24 hours. In each granule, hot plasma rises at the center and sinks at the edges. Magnetic field is collected at the edges of the supergranules as plasma motion can move magnetic field in the photosphere. Sunspots, dark regions in photospheric white light² (Figure 2.6, left), correspond to

² “white light” refers to the integrated visible spectrum emission

regions of concentrated magnetic field. In these locations, magnetic pressure alleviates some of the gas pressure, which lowers the temperature (see numerator of Equation 2.1), and thus the emission peak wavelength and intensity decrease according to Planck’s law (Equation 2.2). These areas are known as active regions when viewed in magnetogram data (Figure 2.6, right) and are the primary source for solar eruptive events (see Section 2.2).

2.1.5 Chromosphere

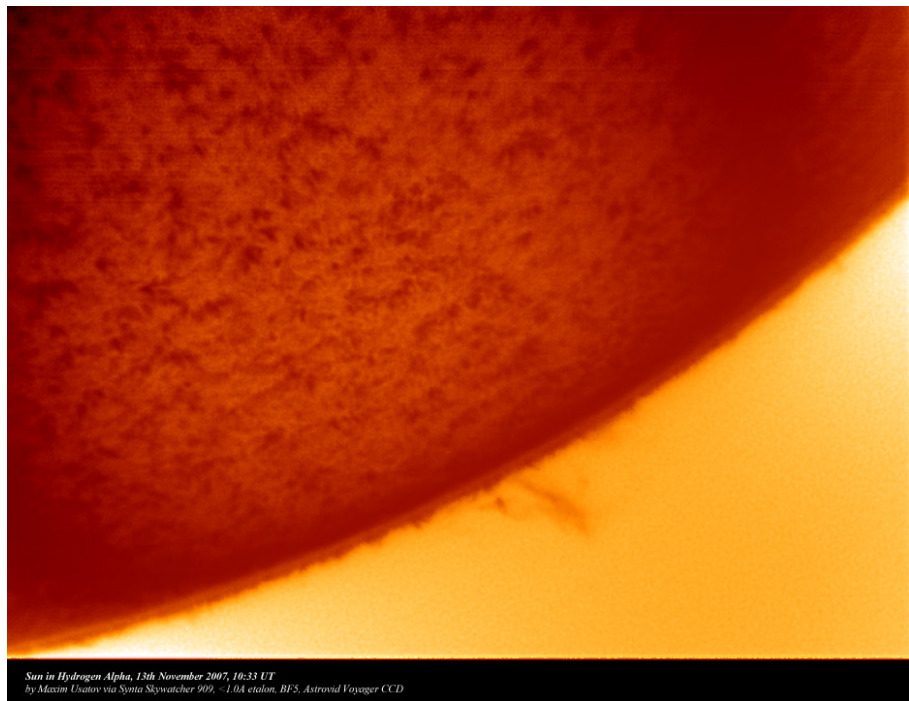


Figure 2.7: Chromospheric spicules visible on the limb³ of the sun, imaged in H α . This photo was taken by an amateur astronomer from the ground, Maxim Usatov.

The chromosphere is an irregular layer of the sun that mostly consists of small jets known as spicules (Figure 2.7). The chromosphere was initially discovered – and only observable – during natural solar eclipses for a few seconds around totality when the bright photosphere was blocked. The layer has a dominant red color, which guided the selection of its name (“chromo” comes from the Greek word for color). The red light comes primarily from H α emission. H α comes from the $n = 3 \rightarrow 2$ transition of hydrogen (Figure 2.8). The next section will go into the details

of electromagnetic radiation, including this type of bound-bound emission. Instruments can use filters to select this particular wavelength, making observation of the chromosphere routine and independent of solar eclipses.

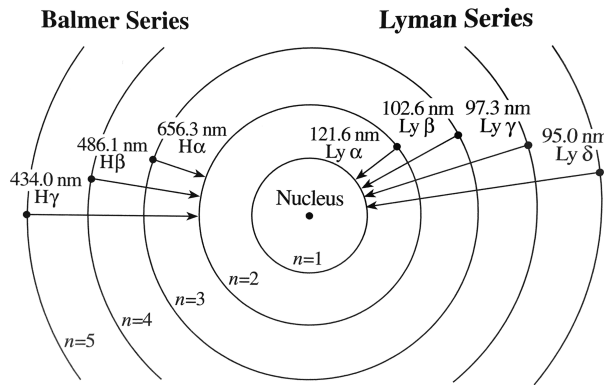


Figure 2.8: Diagram of the hydrogen atom, with electron shells labeled (n). Two important transition series are identified: the Balmer series which includes transitions ending at $n = 2$ and the Lyman series with transitions ending at $n = 1$. The wavelength and common name for the resultant photon emission are also labeled.

2.1.6 Electromagnetic Radiation From Atoms and Charged Particles

There are three basic types of electromagnetic radiation that are emitted by electrons: bound-bound, free-bound, and free-free. Additionally, nuclei can emit photons.

Bound-bound When an electron transitions from one orbital energy of an atom to a lower one, a photon is emitted with energy equal to that of the transition. Downward energy transitions can occur spontaneously or through a collisional de-excitation, where the atom impacts another particle and transfers some of its energy to the other particle. Upward energy transitions can also occur through collision or by absorption of a photon. The wavelength of the emitted photon is primarily determined by the electronic energy transition but can also be influenced by numerous other processes. For example, the strength of the surrounding magnetic field (Zeeman splitting), collisions during the energy transition, and the relative line-of-sight velocity of the atom with respect to the observer (Doppler) all influence the final wavelength of a photon emitted from a

bound-bound transition. These and other effects result in line broadening, sometimes to the point of splitting the lines.

Free-bound Also known as radiative recombination, free-bound transitions are those where an atom captures a free electron. When a free electron is captured, a photon is emitted with energy equal to the difference between the kinetic energy of the free electron and the energy of the bound atomic state. The orbitals of the atom have discrete (quantized) energy values but the kinetic energy of free electrons exists on a continuum. Thus light from free-bound transitions is also a continuum in wavelength though it has a lower limit defined by the energy of the bound state it is captured into. The reverse process (bound-free) is ionization and occurs when a photon is absorbed by an atom and an electron is liberated.

Free-free Also known as Bremsstrahlung (“braking radiation”), any accelerating charged particle emits photons according to Maxwell’s equations. The resultant emission is on a continuum because there are no quantum constraints on the kinetic energy of free particles before or after an acceleration event. Because electrons are much less massive than nuclei, they tend to experience many changes in direction and speed in a dynamic plasma. Even the lightest nucleus – hydrogen, which is just a proton – is 1836 times heavier than an electron. So, while the nucleus will also experience a change in kinetic energy, it is negligible compared to the electron’s. The acceleration in this case is mediated through the powerful electromagnetic force between these oppositely charged particles. It is also possible for the similarly charged ions to accelerate each other, or electrons to accelerate other electrons, but these events are not responsible for the dominant observed emission.

Nuclear decay Nuclei can also be excited into a higher energy state through powerful collisions. When they return to a lower energy state, a photon is emitted and is typically in the gamma range of the spectrum.

2.1.7 Transition Region

The transition region is defined by the rapid increase in temperature between the chromosphere and corona (see Figure 2.2). It is only \sim 100 km thick and is ill defined spatially. Is it in

the spicules of the chromosphere? In the loops of active regions? Its location is not obvious and its existence seems to defy the laws of thermodynamics. The early discovery of how hot the corona was and that the transition region existed was controversial. It depended on temperature-sensitive observations, which have now become routine and widely accepted.

There are several means by which temperature of the solar atmosphere can be inferred. The simplest is the observation of an emission line that has been identified in the laboratory, which specifies the corresponding ion and bound-bound transition. Additional laboratory measurements and theory provide the ionization fraction of each element as a function of temperature (Figure 2.9). A higher temperature results in greater ionization. Thus, observation of an emission line known to correspond to a particular ion is an indicator of that ion's existence in the remote plasma and an approximate temperature can be inferred. Table 2.1 provides some examples for ionization state, corresponding temperature, and a known emission line, which will be used extensively in later chapters.

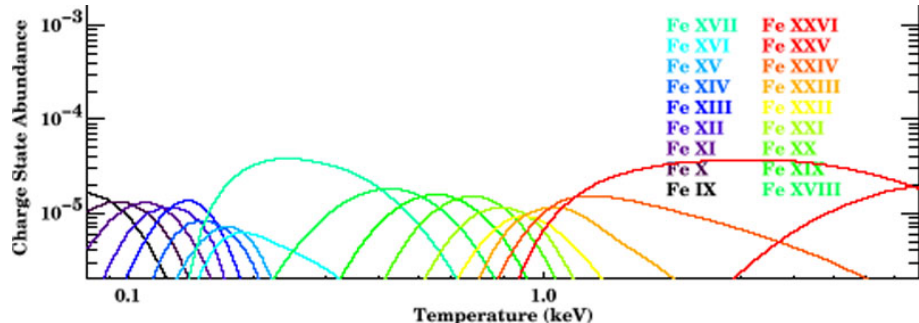


Figure 2.9: Ionization fraction for Fe as a function of energy. Here, energy and temperature are related by a constant value (Boltzmann's constant) and are thus equivalent. Charge state abundance is the product of elemental abundance and ionic fraction. Figure courtesy of Peterson and Fabian (2006).

The next most common method for temperature determination uses the ratio of two emission lines. The flux in each line is dependent on the energy of the bound-bound transition, ΔE , and the collision rates for that transition. The ratio of the line fluxes is temperature sensitive if $\Delta E > k_B T$. This method can handle non-isothermal plasmas by integrating the collision rates over volume. This

Table 2.1: Selected emission lines

Ion	Wavelength (Å)	Peak formation temperature (MK)
Fe IX	171	0.63
Fe X	177	0.93
Fe XI	180	1.15
Fe XII	195	1.26
Fe XIII	202	1.58
Fe XIV	211	1.86
Fe XV	284	2.19
Fe XVI	335	2.69
Fe XVIII	94	6.46
Fe XX	132	9.33

method fails if the lines used have source regions that are distant from each other so care must be taken when the source plasma contains spatial variations in density and temperature, as is the case with the sun. Additionally, this method depends on the relative ion abundances, so if ionization balance varies with time, that time variation must be taken into account. Line ratios are not used for temperature determination in this dissertation.

The mechanism responsible for the rapid temperature change through the transition region remains poorly understood and is one of the biggest problems in solar physics. Theories abound to explain it but are beyond the scope of this dissertation. Here, we simply accept that the transition region *does* lead to a much hotter corona, an observational fact that has long been established.

2.1.8 Thermodynamic Equilibrium

A large, dynamic body such as the sun shouldn't be expected to be in thermodynamic equilibrium everywhere. The term "local thermodynamic equilibrium (LTE)" appreciates this. There are many volumes of the sun where the laws and conveniences of thermodynamic equilibrium can be applied. LTE is a good assumption when three basic criteria are met: the electron and ion

velocity distribution is Maxwellian, the plasma is only weakly ionized such that the Saha equation holds, and collisional excitation dominates radiative such that the Boltzmann equation can be applied.

The Maxwell-Boltzmann equation describes the velocity distribution of a population of particles:

$$f(v) = \sqrt{\left(\frac{m}{2\pi k_B T}\right)^3} 4\pi v^2 e^{-\frac{mv^2}{2k_B T}} \quad (2.3)$$

where f is the probability density function, v is velocity, m is particle mass, and other terms are as previously defined. This is a valid description for processes involving only continuum emission (free-free and free-bound) and is usually valid for atoms and ions in the sun. Particle acceleration during solar flares can push a population of electrons and ions outside of the Maxwellian distribution. The Saha equation describes the ionization state of a plasma as a function of temperature and pressure:

$$\frac{n_{i+1} n_e}{n_i} = \frac{2g_{i+1}}{\Lambda^3 g_i} e^{-\frac{\epsilon_{i+1} - \epsilon_i}{k_B T}} \quad (2.4)$$

where n_i is the number density of ions in the i -th ionization state, n_e is the number density of electrons, Λ is the deBroglie wavelength, g_i is the degeneracy of states for the i -ions, and ϵ_i is the energy to remove i ions from the neutral atom. In the solar atmosphere, the low-lying atomic levels are dominated by radiative ionization while the high levels are dominated by collisional ionization when the temperature and density are high. The Saha equation is valid when collisions dominate the overall plasma or when the radiation field is Planckian (Equation 2.2). The Boltzmann equation (not to be confused with the Maxwell-Boltzmann equation) describes the excitation distribution of electrons in an atom:

$$f(i) = \frac{e^{-\epsilon_i/k_B T}}{\sum_{i=1}^M e^{-\epsilon_i/k_B T}} \quad (2.5)$$

where M is the number of all states accessible to the system and all other terms are as defined previously. The Boltzmann equation is valid when collisions dominate excitation as compared to

radiative excitation. The inherent simplifying assumption is that the excitation state depends only on the temperature and density of the plasma. This is not true in general so the assumption of LTE must be applied carefully. When LTE does hold, the distribution of thermally emitted photons is described by the Planck equation (Equation 2.2). Non-LTE analyses must account for the fact that the radiation field also impacts the population of electrons in atomic energy states.

2.1.9 Corona



Figure 2.10: Composite white-light image of the corona from a total solar eclipse in the Marshall Islands in 2009 July. Features on the moon can be seen in the foreground and a great deal of structure appears in the corona. Image courtesy of Miloslav Druckmuller.

The corona is the highly dynamic, tenuous upper atmosphere of the sun. Its lower boundary is defined by the transition region at approximately 2.45×10^5 km above the photosphere ($1.35 R_\odot$). Its outer boundary is determined by the Alfvén surface where information can no longer be propagated inward and has recently been discovered to be at a much higher altitude than previously thought: 8.35×10^6 km ($12 R_\odot$) above polar coronal holes and 1.04×10^7 km ($15 R_\odot$) at lower latitudes (DeForest et al., 2014). The average temperature of the corona is about 1.5 MK (Figure 2.2) but it ranges from roughly 6.00×10^5 K to 5.00×10^7 K. As mentioned in earlier sections, the ratio of gas to

magnetic pressure, β , is less than 1 in the corona. This is why we see structure in the corona. The magnetic field contorts, compresses, and opens dynamically to produce regions of varying plasma density and temperature (Figure 2.10). Those changes in the plasma impact the electromagnetic emission in terms of the emission line flux and differential emission measure (DEM):

$$F = \frac{2.2 \times 10^{-15}}{4\pi R^2} f A_{el} \int g G(T) Q(T) dT \quad (2.6)$$

$$G(T) = \frac{n_{ion}}{n_{el}} \frac{e^{-h\nu/k_B T}}{\sqrt{T}} \quad (2.7)$$

$$Q(T) = \sum_{i=1}^N \left(\iint_{S_T} \frac{n_e n_i}{|\nabla T|} dS_T \right)_i \quad (2.8)$$

where F is the emission line flux, $G(T)$ is the contribution function, $Q(T)$ is the DEM; R is the distance between the emission and the observer, f is the oscillator strength (probability of absorption/emission between two atomic energy levels), A_{el} is the elemental abundance, g is the Gaunt factor (a correction for absorption/emission to account for quantum effects), ν is photon frequency, S_T is a constant temperature surface, the summation in $Q(T)$ runs across all regions along the line of sight in the temperature range T to $T + \Delta T$, and all other variables are as defined previously. The DEM, and hence the line flux, is strongly dependent on density and moderately dependent on temperature. All of this is to say that where the coronal magnetic field increases the density or temperature of the plasma, the intensity of the emission goes up; thus, images of the corona tend to show bright structures that provide an indicator of magnetic topology and intensity.

The corona is optically thin and as such is not in LTE, i.e., the plasma is not strongly coupled to the locally-generated radiation field. In yet simpler terms, this means that photons generated from a very distant region can stream directly to a plasma parcel of interest and interact there. This makes modeling of the solar atmosphere a nontrivial task. There should be different temperatures defined for photons, electrons, protons, and ions. Their velocities need not be Maxwellian, making the definition of temperature at all somewhat murky. However, many of the emission lines in the corona are emitted by collisionally excited, highly ionized atoms (e.g., Fe IX 171 Å) and these

lines can only be formed above certain temperatures. In regions of the corona that are relatively quiescent, the assumption of a Maxwellian distribution remains a good one, so temperature carries some meaning. Thus, observations of particular emission lines still provide a decent indicator of approximate plasma temperature. Herein, “peak formation temperature” or simply “temperature” will be used as a convenient shorthand that implies the caveats provided above.

2.1.10 Heliosphere

The heliosphere stretches from the end of the corona and encompasses the solar system. It is the region where solar influences dominate the interstellar. Solar wind, a tenuous plasma constantly streaming out from the sun, applies a subtle outward pressure. There are similar breezes coming from the stars. The heliopause is defined as the point of equilibrium between these pressures. The solar wind flows outward at about 400 km/s with a pressure at 1 astronomical unit (AU⁴) in the range of 1×10^{-9} N/m² to 6×10^{-9} N/m². However, this gentle wind is periodically disturbed by spasms in the sun known as solar eruptive events. These events can impact the earth and cause various problems with technology, health, and safety. The physics of solar eruptive events is the subject of Section 2.2 and the impacts and forecasting of space weather is the subject of Section 2.3.

2.2 Physics of Solar Eruptive Events

Solar eruptive events are some of the most energetic phenomena in the solar system. Solar flares can release 6×10^{25} J in minutes to hours – an energy that is hard to fathom. The total world energy consumption over the last 42 years was 1.17×10^{22} J⁵. A powerful flare has more than 5000 times that energy. Coronal mass ejections (CMEs) have a similar amount of energy. The general process for eruptive events is a long period (days or more) of energy storage and then a rapid release of that energy through numerous physical processes. The following subsections

⁴ 1 AU is the average distance between the sun and earth, 1.50×10^8 km

⁵ Analysis based on data from 1971-2013 in International Energy Agency (2015)

provide further detail into energy storage and release.

2.2.1 Magnetic Energy Storage

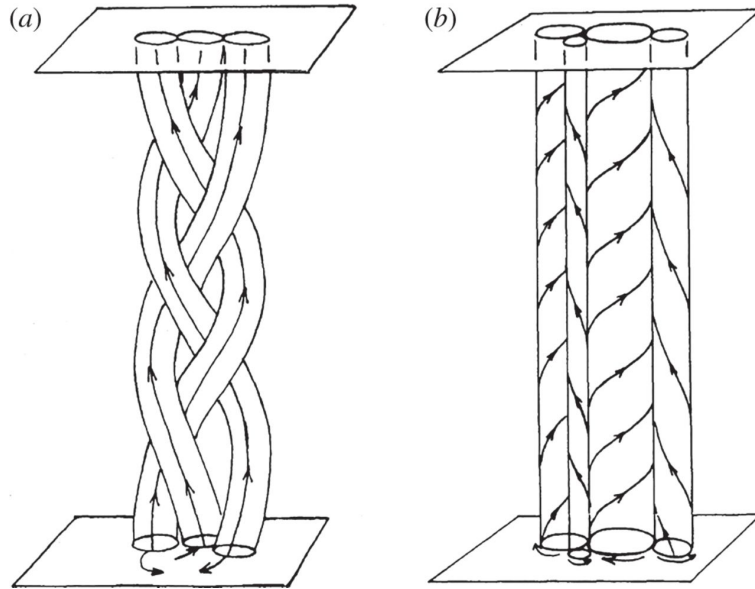


Figure 2.11: Schematic depiction of magnetic energy storage. (Left) Translation of magnetic fields/ropes/strands leads to braiding and tangling and (right) the field lines/ropes/strands can themselves be twisted. Figure courtesy of Klimchuk (2015).

The energy to power a solar eruptive event comes from stored energy in the coronal magnetic field. A “potential” field is defined such that the field is smooth e.g., it has no field lines twisting around each other and instead they nest alongside each other in an orderly way. This is the lowest possible energy configuration of the field, meaning there is no energy to power an eruptive event. When field lines are packed closely together, become braided, shear, or single ropes twist, energy is stored into the field (Figure 2.11). As described earlier, the convective motions at and below the photosphere are one important source of these motions. Additionally, a complex of magnetic fields such as an active region can be influenced by distant eruptive events through energy propagation via the coronal magnetic field, such as Alfvén waves (Schrijver and Title, 2011). Gentler disturbances in the large-scale coronal magnetic field likely occur frequently and could contribute to localized energy concentration.

2.2.2 Energy Release Overview

The rapid energy release of a solar eruptive event is no small topic. As mentioned earlier, worldwide energy consumption pales in comparison to the energy release of a single solar eruptive event and as such, a large number of physical processes are powered. Magnetic reconnection is the widely accepted mechanism that triggers the sudden energy release, though the microphysics remain poorly understood. Magnetic reconnection also occurs in planetary magnetospheres and laboratory experiments have sought to cause it, but the details of this active area of research are beyond the scope of the relevant background to this dissertation. Magnetic energy storage and reconnection is somewhat analogous to the sudden shifting of tectonic plates (earthquakes), avalanches on a ski slope, the snapping of a rubber band that has been twisted too tightly, and the sudden flash and crack of a lightning bolt (Lang, 2001).

As energy continues to build in the coronal magnetic field, eventually somewhere in the complex of loops, a particular strand is stressed beyond a critical limit. Because it can no longer adjust to the additional stress, it suddenly snaps into a new lower-energy configuration as it finds the path of least resistance, like a stream of water working its way through rough downhill terrain. This sudden change to the local field configuration causes the neighboring loops to adjust rapidly as well; in this way the disturbance propagates. Within seconds, all loops in the region are relieving their strain by reducing their twists, shear, and other complexity as they strive toward the nonpotential field configuration. Eventually, a region of loops is reached that are not near their critical stress limit and the propagation ceases. The field configuration after the disturbance contains less energy than before. All of that energy has to go somewhere! It turns out that particle acceleration is one of the key processes powered by this energy release. A comparative few particles can be accelerated to relativistic velocities and/or a huge mass of particles can be accelerated to a few hundred km/s. The former is strongly associated with solar flares (Section 2.2.3) and solar energetic particles (SEPs; not discussed in detail here) while the latter is a simple description of coronal mass ejections (Section 2.2.4). Both are manifestations of magnetic energy release and they can occur

together. Flares are often categorized by the amount of soft x-ray emission they release as measured by the Geostationary Operational Environmental Satellites (GOES) where each letter (A, B, C, M, X) indicates an increased order of magnitude. $\sim 30\%$ of C-class, $\sim 56\%$ of M-class, and $\sim 90\%$ of X-class flares occur with CMEs (Yashiro et al., 2005; Wang and Zhang, 2007). Thus, larger magnitude flares tend to occur with CMEs. The reverse is also true: 90% of the fastest CMEs (> 1500 km/s) are associated with flares while the association rate drops for slower CMEs (Wang and Zhang, 2008).

2.2.3 Solar Flares

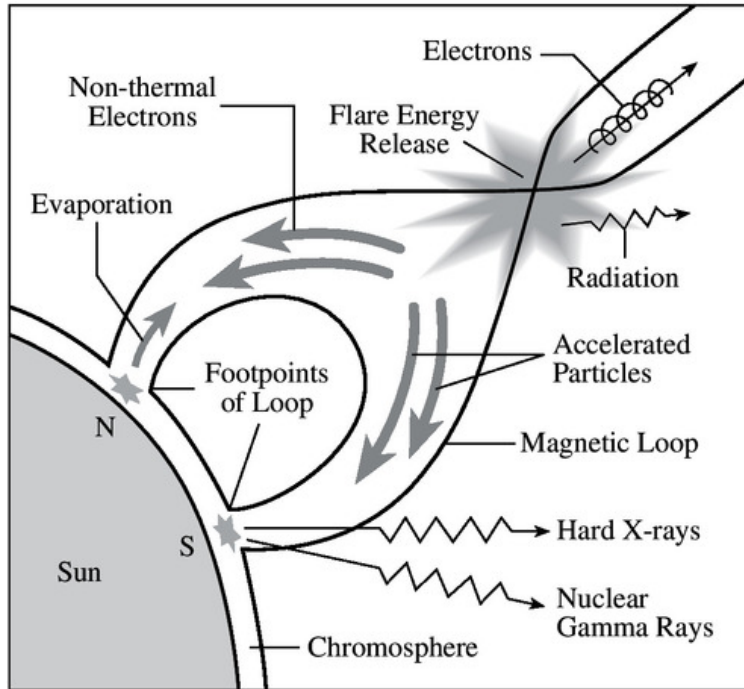


Figure 2.12: Schematic depiction of solar flare energy release processes. Figure courtesy of Lang (2001).

“Solar flare” is a somewhat vague term that broadly encompasses all of the rapid magnetic energy release processes that result in electromagnetic radiation (Figure 2.12). One natural place for some of the energy to go is Joule heating. This is a process where electrons are accelerated by an electric field and collide with relatively stationary ions causing them to scatter randomly

(though still in a Maxwellian distribution), thus increasing the average kinetic energy of the system (i.e., heating). Particle acceleration in flares is poorly understood but there are numerous proposed mechanisms that could produce electron and ion beams. Each proposed mechanism has issues and the existing observations have not placed sufficient constraints to determine which mechanism dominates for various physical conditions (Kontar et al., 2011; Zharkova et al., 2011). The observations do tell us that acceleration occurs near or above the top of the coronal loops. Some particles are accelerated outward (SEPs) and others are accelerated downward.

Electrons and ions that are accelerated downward are trapped by magnetic field because $\beta < 1$, so they run down the legs of the coronal loops until they reach the relatively dense chromosphere. At this point, numerous physical processes ignite. As the non-thermal⁶ charged particles in the beam approach the plasma in the chromosphere, their electromagnetic attraction/repulsion causes acceleration, which results in bremsstrahlung continuum radiation. Sometimes the particles in the beam collide with the chromospheric particles, which results in direct heating, ionization, atomic excitation of electrons, and atomic excitation of the nucleus. Electrons that become excited but remain bound may then spontaneously decay in a bound-bound transition by emitting a photon (often in SXR or EUV). Alternatively, the excited atom may collisionally de-excite – another heating mechanism. Heating in the chromosphere causes the plasma to rapidly expand and because $\beta < 1$, it expands up the legs of the coronal loops. Those loops then appear bright in SXR and EUV wavelengths (Figure 2.13). These processes tend to generate a multitude of high energy emission, from UV to gamma, and also microwave emission at the characteristic plasma frequency as the electron beam causes a small oscillation in the elements of the target plasma. Because the corona is optically thin, we are able to directly observe these emissions.

The HXRs and microwave emission tend to cease within minutes as the electron beam stops. The period that these emissions persist is known as the impulsive phase of the flare. The gradual phase is essentially the atmospheric response to the disturbance of the impulsive phase; the hot plasma (upwards of 50 MK) cools and lower ionization states see an enhancement. Those lower

⁶ Non-thermal implies that the velocity distribution is not Maxwellian

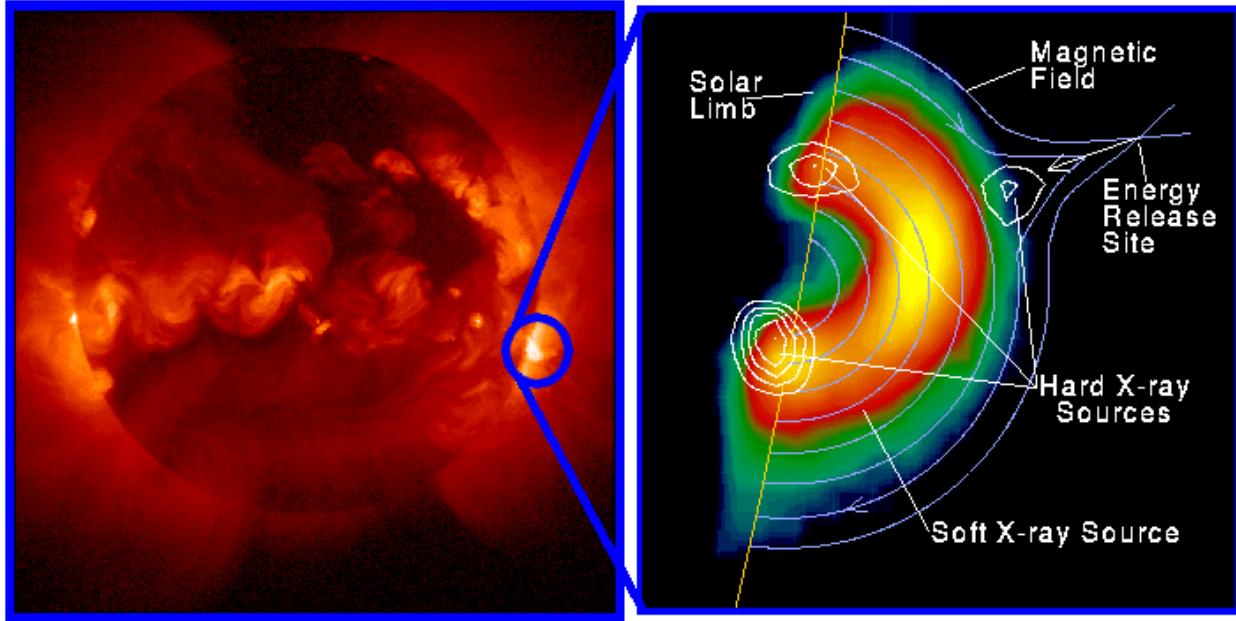


Figure 2.13: (Left) SXR image of the sun during a flare on 1992 January 13. (Right) The flaring loops in SXR and HXR wavelengths. Images from instruments onboard the Yohkoh spacecraft. Figure courtesy of Holman (2008).

ionization states radiate, which makes them observable and contributes to the cooling of the plasma.

Highly relevant to the following chapters, many of the gradual phase emission lines are in the EUV.

2.2.4 Coronal Mass Ejections

Energy stored in the coronal magnetic field can also be directed into accelerating a great mass out of the corona and into the heliosphere. Prior to the eruption, the strong magnetic fields of the active region in a low β environment can prevent a great mass of plasma from escaping, despite strong outward plasma pressure. The sudden reconfiguration of the magnetic field changes that situation: the restraining magnetic field can be disconnected from lower down, effectively pinching off a magnetic bubble (Figure 2.14). Often times, highly-stable plasma features can be found resting in regions of strong magnetic field, which tend to be in and near active regions (Figure 2.14). These features are called filaments when seen on disk because they appear dark, and prominences when viewed towering over the solar limb. Filaments/prominences have orders of magnitude higher

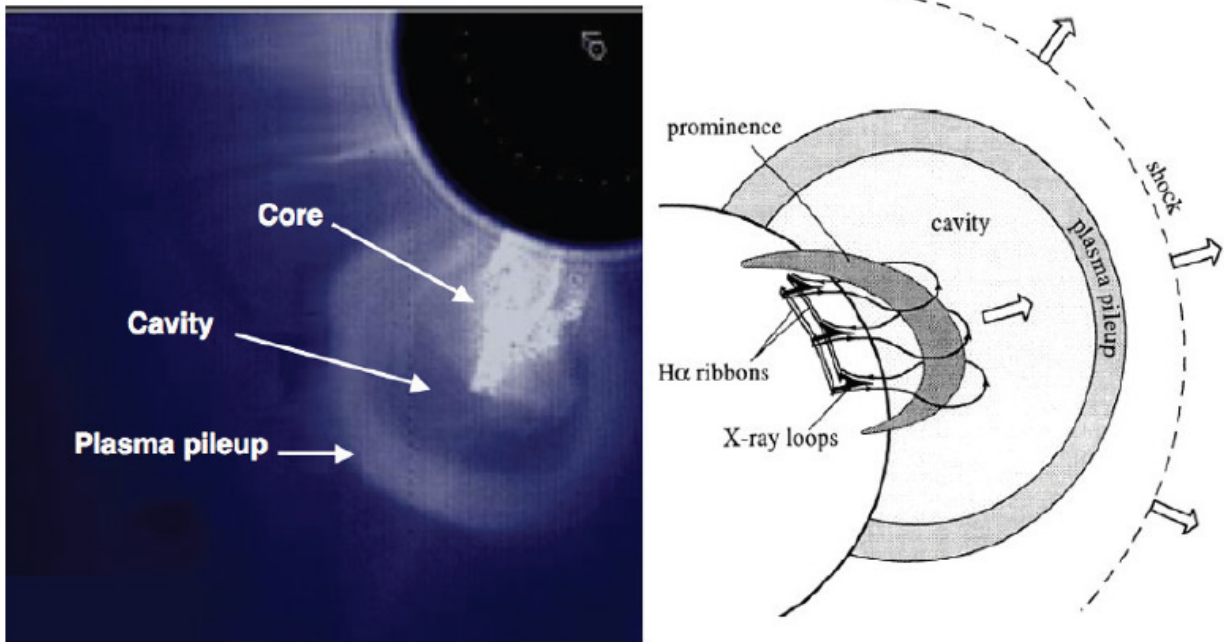


Figure 2.14: (Left) Typical observation of a CME. (Right) Schematic depiction of filament eruption CME. Figure courtesy of Forbes (2000).

density than their surroundings but are at orders of magnitude lower temperature. They should sink like a brick in water or evaporate like an ice cube in an oven but they are supported and protected by the strong magnetic fields encapsulating them. When a CME departs, often times a filament/prominence that was a part of the local magnetic structure will be torn away with it. This adds to the mass of the CME and can make for beautiful images (Figure 2.15). Here too, the precise mechanism for accelerating the CME is poorly understood. It is particularly perplexing because the average speed of a CME is 400 km/s but the escape velocity here is about 600 km/s. What is relevant for this dissertation is that as the CME leaves, it brings its emission with it, leaving a temporary void in the corona. “Transient coronal holes” are now known as coronal dimmings and these will be the focus of Chapters 3-5.



Figure 2.15: Prominence eruption as viewed from the Solar Dynamics Observatory’s Atmospheric Imaging Assembly. Image credit: NASA.

2.3 Space Weather

If solar eruptive events are directed toward Earth, there can be myriad negative consequences (National Research Council, 2008), which provides some practical motivation to study the responsible events beyond their merits as scientific curiosities. The National Research Council (2008) report is the definitive source for space weather impacts so only a few examples will be listed here. The electromagnetic radiation from solar flares is absorbed by the earth’s atmosphere, which can cause it to expand. Satellites at a particular altitude will then see a greater number of particles in their path and thus experience a small but non-negligible increase to their drag. The gross effect is that the orbital lifetime of satellites in low Earth orbit is reduced, unless they have the capability to boost themselves as the International Space Station does periodically. Additionally, high energy photons, electrons, and protons can be directly absorbed by satellites or humans in space. This can

cause numerous problems with electronics and health. In particular, solar storms can cause disruptions to the global positioning satellite (GPS) system. This is an inconvenience to people on travel in unfamiliar places, but has serious implications for the agricultural and drilling industries that increasingly rely on GPS for precise positioning in their automated systems. Coronal mass ejections are clouds of electrically charged plasma that influence the earth's magnetosphere. According to Maxwell's equations, a changing magnetic field induces a current. Long oil pipelines and power lines are particularly susceptible to this because they are good electrical conductors. In the case of power lines, the surges in current can exceed the limits of tolerance on large transformers and blow them out. These transformers are expensive and have long lead times to replace; thus large populations can be left without power for extended periods of time, as was the case in Quebec in 1989. Finally, the earth's ionosphere can be influenced by solar eruptive events, causing disruptions in radio communication that rely on the ionosphere to bounce signals over long distances. This has important implications for the airline industry because airplanes are required to maintain constant contact with the ground. In relatively inaccessible areas like the poles and the oceans, they rely on the ionosphere to maintain contact. Thus, when ionospheric disturbance disrupt an airlines ability to maintain contact, they are forced to reroute flights. Many of the human implications of space weather can be mitigated with warning. For example, astronauts can take shelter, satellites can be temporarily powered down or put into safe mode, and transformers can be protected from current surges.

It remains difficult to predict when solar eruptive events will occur. One popular method uses photospheric magnetic field measurements to derive parameters tied to field complexity (e.g., emerging flux, polarity inversion line length, magnetic field gradients), which are proxies for the amount of stored energy in the magnetic field. These data are then used to make forecasts of solar flares but while they show a positive correlation to solar flare occurrence and magnitude, they have not proven particularly effective for real-time prediction (Mason and Hoeksema, 2010). Fortunately, CMEs are the more geoeffective type of solar eruptive event and they take several hours to a few days to reach 1 AU. This makes nowcasting possible because the light from CMEs only takes 8

minutes to reach the same distance. An industry has sprung up around the monitoring of real-time data from various space-weather assets, and they issue alerts to other industries that may be impacted. The true test of any science is its ability to make accurate and precise predictions. The sun may be the most well studied star in the universe, but there remains ample room for improvement in our understanding of its details and our observations of it.

2.4 Instrument Descriptions

The following subsections are broken into instrument types. Only instruments that are important for this dissertation are described. Of primary importance is the Solar Dynamics Observatory's Extreme Ultraviolet Variability Experiment spectrograph, so it will be described first.

2.4.1 Spectrographs

The Extreme Ultraviolet (EUV) Variability Experiment (EVE; Woods et al. 2012) onboard the Solar Dynamics Observatory (SDO; Pesnell et al. 2012) was launched on 2010 February 11 into a geosynchronous orbit that has a view of the sun that is only occasionally obstructed by the earth. EVE is a suite of instruments that measure EUV emission from the sun (Figure 2.16). Of primary interest to this dissertation is the Multiple EUV Grating Spectrographs (MEGS)-A, which is a grazing-incidence spectrograph that obtains 1 Å resolution spectra from 50 to 370 Å every 10 seconds. This range contains all of the emission lines listed in Table 2.1, which are imaged on two charge coupled devices (CCDs), thus reducing cross-calibration concerns to a near minimum. The spectral resolution is sufficiently high that emission line blends are few and do not impact the analyses to come in the following chapters. However, as an irradiance instrument, EVE has no spatial resolution.

The modified Amptek X123 silicon drift detector onboard MinXSS is a spectrometer to observe SXRs. It will be described in Chapter 6.

2.4.2 Spectral Imagers

Also onboard SDO is the Atmospheric Imaging Assembly (AIA; Lemen et al. 2012). AIA consists of seven EUV channels from four telescopes. The full solar disk is observed and the light is imaged onto 4096 x 4096 CCDs every 12 seconds. The spatial resolution of 1.5 arcsec translates to about 1000 km at the sun. AIA uses filters to select bandpasses, most of which are in the EUV and complement EVE data. The filters have bandpasses that are several nanometers wide, which results in spectral line blending. Spectral-line blends in this case result in degeneracy in temperature space. For example, if a pixel in the 171 Å bandpass becomes bright, it is not known if that is due to an enhancement in Fe IX or Fe X. The sharpness of the 171 Å bandpass helps mitigate this issue, but as can be seen in Figure 2.16, some of the bandpasses cover a wide range of wavelengths, which can make temperature diagnostics difficult. Fortunately, analyses can leverage AIA and EVE data together to gain an improved understanding of solar plasma in terms of space, time, and temperature.

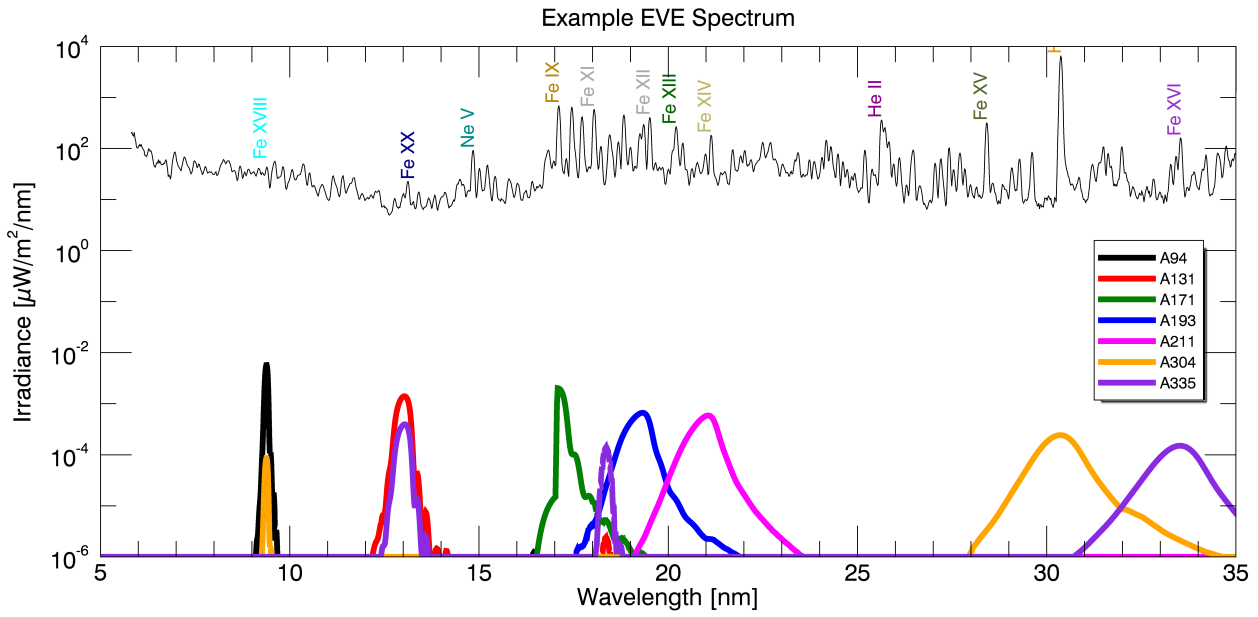


Figure 2.16: The AIA bandpasses with an example EVE solar spectrum to provide an idea of the amount of blending. Some emission lines are labeled with their corresponding ion.

2.4.3 Coronagraphs

Coronagraphs are instruments that block out the bright photosphere to observe the corona, just as rare total solar eclipses do. The Solar and Heliospheric Observatory (SOHO; Domingo et al. 1995) has a coronagraph onboard – the Large Angle Spectroscopic Coronagraph (LASCO; Brueckner et al. 1995). SOHO was launched 1995 December 2 to the Earth-Sun first Lagrange point, which is always between the earth and sun (though still much closer to the earth). LASCO contains three coronagraphs with different fields of view. Only C2 (1.5 - 6 R_☉) and C3 (3.7 - 30 R_☉) have remained in operation through the present era when SDO became available. LASCO and other coronagraphs observe white light from the corona that has been Thomson scattered by the numerous electrons in the fully-ionized and hydrogen-dominated corona. This makes them ideal for observing coronal mass ejections.

The Solar Terrestrial Relations Observatory (STEREO; Kaiser et al. 2007) contains an instrument similar to LASCO, two Lyot coronagraphs (COR1 and COR2; Howard et al. 2008). COR1 has a field of view from 1.5 - 4 R_☉ and COR2 from 2.5 - 15 R_☉. The STEREO mission has two identical spacecraft that were launched on 2006 October 26; one is slightly inside Earth’s orbit and thus travels further and further ahead of the earth, and the other is slightly outside Earth’s orbit so falls behind the Earth. The increasing distance to these spacecraft means the communications bandwidth is always diminishing, so the resolution and cadence of COR and the other instruments could not be as high as the imaging technology at the time could have made them. Nevertheless, the instruments onboard STEREO provide truly unique possibilities for data analysis. In particular, the geometry of CMEs can be better determined by using STEREO/COR in conjunction with each other and/or with LASCO. This means that CME direction can be determined less ambiguously and thus a “true-space” velocity computed.

Bibliography

- Acton, L. W., Weston, D. C., and Bruner, M. E. (1999). Deriving solar X ray irradiance from Yohkoh observations. *Journal of Geophysical Research*, 104(A7):14827.
- Andretta, V., Del Zanna, G., and Jordan, S. D. (2003). The EUV helium spectrum in the quiet Sun: A by-product of coronal emission? *Astronomy and Astrophysics*, 400(2):737–752.
- Arp, U., Clark, C., Deng, L., Faradzhev, N., Farrell, A., Furst, M., Grantham, S., Hagley, E., Hill, S., Lucatorto, T., Shaw, P.-S., Tarrio, C., and Vest, R. (2011). SURF III: A flexible synchrotron radiation source for radiometry and research. *Nuclear Instruments and Methods in Physics Research Section A: Accelerators, Spectrometers, Detectors and Associated Equipment*, 649(1):12–14.
- Aschwanden, M. J. (2009). 4-D modeling of CME expansion and EUV dimming observed with STEREO/EUVI. *Annales Geophysicae*, 27(8):3275–3286.
- Aschwanden, M. J., Nitta, N. V., Wuelser, J.-P., Lemen, J. R., Sandman, A., Vourlidas, A., and Colaninno, R. C. (2009a). First Measurements of the Mass of Coronal Mass Ejections From the EUV Dimming Observed With Stereo EUVI A + B Spacecraft. *The Astrophysical Journal*, 706(1):376–392.
- Aschwanden, M. J., Wuelser, J. P., Nitta, N. V., and Lemen, J. R. (2009b). Solar Flare and CME Observations with STEREO/EUVI. *Solar Physics*, 256(1-2):3–40.
- Attrill, G. D. R., Harra, L. K., van Driel-Gesztelyi, L., and Wills-Davey, M. J. (2010). Revealing the Fine Structure of Coronal Dimmings and Associated Flows with Hinode/EIS. *Solar Physics*, 264(1):119–147.
- Bailey, S. M., Woods, T. N., Barth, C. A., Solomon, S. C., Canfield, L. R., and Korde, R. (2000). Measurements of the solar soft X-ray irradiance by the Student Nitric Oxide Explorer : First analysis and underflight calibrations. *Journal of Geophysical Research*, 105:27179–193.
- Baker, D. N., Jaynes, A. N., Hoxie, V. C., Thorne, R. M., Foster, J. C., Li, X., Fennell, J. F., Wygant, J. R., Kanekal, S. G., Erickson, P. J., Kurth, W., Li, W., Ma, Q., Schiller, Q., Blum, L., Malaspina, D. M., Gerrard, A., and Lanzerotti, L. J. (2014). An impenetrable barrier to ultrarelativistic electrons in the Van Allen radiation belts. *Nature*, 515(7528):531–4.
- Bein, B. M., Temmer, M., Vourlidas, A., Veronig, A. M., and Utz, D. (2013). THE HEIGHT EVOLUTION OF THE TRUE CORONAL MASS EJECTION MASS DERIVED FROM STEREO COR1 AND COR2 OBSERVATIONS. 31.

- Bevington, P. (2003). Data reduction and error analysis for the physical sciences. McGraw-Hill, Boston.
- Bewsher, D., Harrison, R. A., and Brown, D. S. (2008). The relationship between EUV dimming and coronal mass ejections I. Statistical study and probability model. Astronomy & Astrophysics, 478:897–906.
- Blum, L. and Schiller, Q. (2012). Characterization and Testing of an Energetic Particle Telescope for a CubeSat Platform.
- Blum, L. W., Schiller, Q., Li, X., Millan, R., Halford, A., and Woodger, L. (2013). New conjunctive CubeSat and balloon measurements to quantify rapid energetic electron precipitation. Geophysical Research Letters, 40(22):5833–5837.
- Brueckner, G. E., Howard, R. A., Koomen, M. J., Korendyke, C. M., Michels, D. J., Moses, J. D., Socker, D. G., Dere, K. P., Lamy, P. L., Llebaria, A., Bout, M. V., Schwenn, R., Simnett, G. M., Bedford, D. K., and Eyles, C. J. (1995). The Large Angle Spectroscopic Coronagraph. Solar Physics, 162:357–402.
- Caspi, A. and Lin, R. P. (2010). RHESSI Line and Continuum Observations of Super-hot Flare Plasma. The Astrophysical Journal, 725:L161–166.
- Caspi, A., McTiernan, J. M., and Warren, H. P. (2014). CONSTRAINING SOLAR FLARE DIFFERENTIAL EMISSION MEASURES WITH EVE AND RHESSI. The Astrophysical Journal, 788(2):L31.
- Caspi, A., Woods, T. N., and Warren, H. P. (2015). New Observations of the Solar 0.55 Kev Soft X-Ray Spectrum. The Astrophysical Journal, 802(1):L2.
- Chamberlin, P. C., Woods, T. N., and Eparvier, F. G. (2007). Flare Irradiance Spectral Model (FISM): Daily component algorithms and results. Space Weather, 5(7):n/a–n/a.
- Chamberlin, P. C., Woods, T. N., and Eparvier, F. G. (2008). Flare Irradiance Spectral Model (FISM): Flare component algorithms and results. Space Weather, 6(5):n/a–n/a.
- Chamberlin, P. C., Woods, T. N., Eparvier, F. G., and Jones, A. R. (2009). <title>Next generation x-ray sensor (XRS) for the NOAA GOES-R satellite series</title>. In Fineschi, S. and Fennelly, J. A., editors, SPIE Optical Engineering + Applications, pages 743802–743802–10. International Society for Optics and Photonics.
- Chen, P. F., Fang, C., and Shibata, K. (2005). A Full View of EIT Waves. The Astrophysical Journal, 622(2):1202–1210.
- Chen, P. F., Wu, S. T., Shibata, K., and Fang, C. (2002). Evidence of EIT and Moreton Waves in Numerical Simulations. The Astrophysical Journal, 572(1):L99–L102.
- Christensen-Dalsgaard, J., Dappen, W., Ajukov, S. V., Anderson, E. R., Antia, H. M., Basu, S., Baturin, V. A., Berthomieu, G., Chaboyer, B., Chitre, S. M., Cox, A. N., Demarque, P., Donatowicz, J., Dziembowski, W. A., Gabriel, M., Gough, D. O., Guenther, D. B., Guzik, J. A., Harvey, J. W., Hill, F., Houdek, G., Iglesias, C. A., Kosovichev, A. G., Leibacher, J. W., Morel, P., Proffitt, C. R., Provost, J., Reiter, J., Rhodes, E. J., Rogers, F. J., Roxburgh, I. W., Thompson, M. J., and Ulrich, R. K. (1996). The Current State of Solar Modeling. Science, 272(5266):1286–1292.

- Colaninno, R. C. and Vourlidas, A. (2009). First Determination of the True Mass of Coronal Mass Ejections: A Novel Approach To Using the Two Stereo Viewpoints. *The Astrophysical Journal*, 698:852–858.
- Colaninno, R. C., Vourlidas, A., and Wu, C. C. (2013). Quantitative comparison of methods for predicting the arrival of coronal mass ejections at Earth based on multiview imaging. *Journal of Geophysical Research: Space Physics*, 118(11):6866–6879.
- DeForest, C. E., Howard, T. A., and McComas, D. J. (2014). Inbound Waves in the Solar Corona: A Direct Indicator of Alfvén Surface Location. *The Astrophysical Journal*, 787(2):124.
- Dere, K. P., Landi, E., Mason, H. E., Monsignori Fossi, B. C., and Young, P. R. (1997). CHIANTI - an atomic database for emission lines. *Astronomy and Astrophysics Supplement Series*, 125:149–173.
- Domingo, V., Fleck, B., and Poland, A. I. (1995). The SOHO mission: An overview. *Solar Physics*, 162(1-2):1–37.
- Doschek, G. A. (1990). Soft X-ray spectroscopy of solar flares - an overview. *The Astrophysical Journal Supplement Series*, 73:117.
- Eddy, J. A. (1979). *A New Sun: The Solar Results from Skylab*. National Aeronautics and Space Administration, Washington, D. C.
- Fletcher, L., Dennis, B. R., Hudson, H. S., Krucker, S., Phillips, K., Veronig, A. M., Battaglia, M., Bone, L., Caspi, A., Chen, Q., Gallagher, P. T., Grigis, P. T., Ji, H., Liu, W., Milligan, R. O., and Temmer, M. (2011). An Observational Overview of Solar Flares. *Space Science Reviews*, 159(1-4):19–106.
- Forbes, T. G. (2000). A review on the genesis of coronal mass ejections. *Journal of Geophysical Research: Space Physics*, 105(A10):23153–23165.
- Gary, G. A. (2001). Plasma Beta above a Solar Active Region: Rethinking the Paradigm. *Solar Physics*, 203(1):71–86.
- Gerhardt, D. (2010). Passive Magnetic Attitude Control for CubeSat Spacecraft.
- Gerhardt, D. and Palo, S. (2016a). Volume Magnetization for System-Level Testing of Magnetic Materials within Small Satellites.
- Gerhardt, D. and Palo, S. E. (2016b). Passive Magnetic Attitude Control Settling Prediction with On-Orbit Verification using the Colorado Student Space Weather Experiment CubeSat.
- Gerhardt, D., Palo, S. E., Schiller, Q., Blum, L., Li, X., and Kohnert, R. (2013). The Colorado Student Space Weather Experiment (CSSWE) On-Orbit Performance. *Journal of Small Satellites*, 3(1):265–281.
- Gilbert, H. R., Inglis, a. R., Mays, M. L., Ofman, L., Thompson, B. J., and Young, C. a. (2013). Energy Release From Impacting Prominence Material Following the 2011 June 7 Eruption. *The Astrophysical Journal*, 776(1):L12.
- Giordano, S., Antonucci, E., and Dodero, M. (2000). OXYGEN VELOCITIES IN A POLAR CORONAL. *Advances in Space Research*, 25(9):1927–1930.

- Gopalswamy, N., Yashiro, S., Michalek, G., Stenborg, G., Vourlidas, A., L, F. S., and Howard, R. A. (2009). The SOHO / LASCO CME Catalog. *Earth Moon Planet*, 104:295–313.
- Greenstein, J. L. (1958). High-Resolution Spectra of Comet MRKOS. *The Astrophysical Journal*, 128:106.
- Harra, L. K., Mandrini, C. H., Dasso, S., Gulisano, A. M., Steed, K., and Imada, S. (2010). Determining the Solar Source of a Magnetic Cloud Using a Velocity Difference Technique. *Solar Physics*, 268(1):213–230.
- Harra, L. K. and Sterling, A. C. (2001). Material Outflows from Coronal Intensity "Dimming Regions" During Coronal Mass Ejection Onset. *The Astrophysical Journal Letters*, 561:215–218.
- Harrison, R. A., Bryans, P., Simnett, G. M., and Lyons, M. (2003). Coronal dimming and the coronal mass ejection onset. *Astronomy & Astrophysics*, 400:1071–1083.
- Harrison, R. A. and Lyons, M. (2000). A spectroscopic study of coronal dimming associated with a coronal mass ejection. *Astronomy & Astrophysics*, 1108:1097–1108.
- Holman, G. (2008). Overview of Solar Flares.
- Howard, R. A., Moses, J. D., Vourlidas, A., Newmark, J. S., Socker, D. G., Plunkett, S. P., Korendyke, C. M., Cook, J. W., Hurley, A., Davila, J. M., Thompson, W. T., St. Cyr, O. C., Mentzell, E., Mehalick, K., Lemen, J. R., Wuelser, J. P., Duncan, D. W., Tarbell, T. D., Wolfson, C. J., Moore, A., Harrison, R. A., Waltham, N., Lang, J., Davis, C. J., Eyles, C. J., Mapson-Menard, H., Simnett, G. M., Halain, J. P., Defise, J. M., Mazy, E., Rochus, P., Mercier, R., Ravet, M. F., Delmotte, F., Auchere, F., Delaboudiniere, J. P., Bothmer, V., Deutsch, W., Wang, D., Rich, N., Cooper, S., Stephens, V., Maahs, G., Baugh, R., McMullin, D., and Carter, T. (2008). Sun Earth Connection Coronal and Heliospheric Investigation (SECCHI). *Space Science Reviews*, 136(1-4):67–115.
- Hudson, H. S., Lemen, J. R., St. Cyr, O. C., Sterling, A. C., and Webb, D. F. (1998). X-ray coronal changes during halo CMEs. *Geophysical Research Letters*, 25(14):2481–2484.
- Hudson, H. S., Woods, T. N., Chamberlin, P. C., Fletcher, L., Zanna, G. D., Didkovsky, L., Labrosse, N., and Graham, D. (2011). The EVE Doppler Sensitivity and Flare Observations. *Solar Physics*, 273:69–80.
- Hyder, C. L. and Lites, B. W. (1970). H-alpha Doppler Brightening and Lyman-alpha Doppler Dimming in Moving H-alpha Prominences. *Solar Physics*, 14(1):147–156.
- Imada, S., Hara, H., Watanabe, T., Kamio, S., Asai, A., Matsuzaki, K., Harra, L. K., and Mariska, J. T. (2007). Discovery of a Temperature-Dependent Upflow in the Plage Region during a Gradual Phase of the X-Class Flare. *Publications of the Astronomical Society of Japan*, 59(sp3):S793–S799.
- International Energy Agency (2015). 2015 Key World Energy Statistics. Technical report, International Energy Agency.
- Jaynes, A. N., Li, X., Schiller, Q. G., Blum, L. W., Tu, W., Turner, D. L., Ni, B., Bortnik, J., Baker, D. N., Kanekal, S. G., Blake, J. B., and Wygant, J. (2014). Evolution of relativistic outer belt electrons during an extended quiescent period. *Journal of Geophysical Research: Space Physics*, 119(12):9558–9566.

- Jin, M., Ding, M. D., Chen, P. F., Fang, C., and Imada, S. (2009). CORONAL MASS EJECTION INDUCED OUTFLOWS OBSERVED WITH HINODE /EIS. *The Astrophysical Journal*, 702(1):27–38.
- Kahler, S. (1992). Solar Flares and Coronal Mass Ejections. *Annual Review of Astronomy and Astrophysics*, 30:113–141.
- Kahler, S. W. (1982). The role of the big flare syndrome in correlations of solar energetic proton fluxes and associated microwave burst parameters. *Journal of Geophysical Research*, 87(A5):3439.
- Kaiser, M. L., Kucera, T. A., Davila, J. M., St. Cyr, O. C., Guhathakurta, M., and Christian, E. (2007). The STEREO Mission: An Introduction. *Space Science Reviews*, 136(1-4):5–16.
- Klimchuk, J. A. (2006). On Solving the Coronal Heating Problem. *Solar Physics*, 234(1):41–77.
- Klimchuk, J. A. (2015). Key aspects of coronal heating. *Philosophical transactions. Series A, Mathematical, physical, and engineering sciences*, 373(2042):20140256.
- Kohnert, R., Palo, S., and Li, X. (2011). Small Space Weather Research Mission Designed Fully by Students. *Space Weather*, 9(4):n/a–n/a.
- Kontar, E. P., Brown, J. C., Emslie, A. G., Hajdas, W., Holman, G. D., Hurford, G. J., Kašparová, J., Mallik, P. C. V., Massone, A. M., McConnell, M. L., Piana, M., Prato, M., Schmahl, E. J., and Suarez-Garcia, E. (2011). Deducing Electron Properties from Hard X-ray Observations. *Space Science Reviews*, 159(1-4):301–355.
- Krista, L. D. and Reinard, A. (2013). STUDY OF THE RECURRING DIMMING REGION DETECTED AT AR 11305 USING THE CORONAL DIMMING TRACKER (CoDiT). *The Astrophysical Journal*, 762(2):91.
- Labrosse, N. and Mcglinchey, K. (2012). Plasma diagnostic in eruptive prominences from SDO / AIA observations at 304 Å. *Astronomy & Astrophysics*, 537:A100.
- Landi, E., Del Zanna, G., Young, P. R., Dere, K. P., Mason, H. E., and Landini, M. (2006). CHIANTIAn Atomic Database for Emission Lines. VII. New Data for XRays and Other Improvements. *The Astrophysical Journal Supplement Series*, 162:261–280.
- Lang, K. R. (2001). The Cambridge Encyclopedia of the Sun. *The Cambridge Encyclopedia of the Sun*.
- Lemen, J. R., Title, A. M., Akin, D. J., Boerner, P. F., Chou, C., Drake, J. F., Duncan, D. W., Edwards, C. G., Friedlaender, F. M., Heyman, G. F., Hurlburt, N. E., Katz, N. L., Kushner, G. D., Levay, M., Lindgren, R. W., Mathur, D. P., Mcfeaters, E. L., Mitchell, S., Rehse, R. A., Schrijver, C. J., Springer, L. A., Stern, R. A., Tarbell, T. D., Wolfson, C. J., Yanari, C., Bookbinder, J. A., Cheimets, P. N., Caldwell, D., Deluca, E. E., Gates, R., Golub, L., Park, S., Podgorski, W. A., Bush, R. I., Scherrer, P. H., Gummin, M. A., Smith, P., Auker, G., Jerram, P., Pool, P., Souffri, R., Windt, D. L., Beardsley, S., Clapp, M., Lang, J., and Waltham, N. (2012). The Atmospheric Imaging Assembly (AIA) on the Solar Dynamics Observatory (SDO). *Solar Physics*, 275:17–40.
- Li, X., Palo, S., Kohnert, R., Blum, L., Gerhardt, D., Schiller, Q., and Califf, S. (2013a). Small Mission Accomplished by Students-Big Impact on Space Weather Research. *Space Weather*, 11(2):55–56.

- Li, X., Palo, S., Kohnert, R., Gerhardt, D., Blum, L., Schiller, Q., Turner, D., Tu, W., Sheiko, N., and Cooper, C. S. (2012). Colorado Student Space Weather Experiment: Differential Flux Measurements of Energetic Particles in a Highly Inclined Low Earth Orbit. In Summers, D., Mann, I. R., Baker, D. N., and Schulz, M., editors, *Dynamics of the Earth's Radiation Belts and Inner Magnetosphere*, Geophysical Monograph Series, pages 385–411, Washington, D. C. American Geophysical Union.
- Li, X., Schiller, Q., Blum, L., Califf, S., Zhao, H., Tu, W., Turner, D. L., Gerhardt, D., Palo, S., Kanekal, S., Baker, D. N., Fennell, J., Blake, J. B., Looper, M., Reeves, G. D., and Spence, H. (2013b). First results from CSSWE CubeSat: Characteristics of relativistic electrons in the near-Earth environment during the October 2012 magnetic storms. *Journal of Geophysical Research: Space Physics*, 118(10):6489–6499.
- Li, X., Selesnick, R. S., Baker, D. N., Jaynes, A. N., Kanekal, S. G., Schiller, Q., Blum, L., Fennell, J., and Blake, J. B. (2015). Upper limit on the inner radiation belt MeV electron intensity. *Journal of geophysical research. Space physics*, 120(2):1215–1228.
- Lin, R. P., Dennis, B. R., Hurford, G. J., Smith, D. M., Zehnder, A., Harvey, P. R., Curtis, D. W., Pankow, D., Turin, P., Bester, M., Csillaghy, A., Lewis, M., Madden, N., Beek, H. F., Appleby, M., Raudorf, T., McTiernan, J., Ramaty, R., Schmahl, E., Schwartz, R., Krucker, S., Abiad, R., Quinn, T., Berg, P., Hashii, M., Sterling, R., Jackson, R., Pratt, R., Campbell, R. D., Malone, D., Landis, D., Cork, C., Tolbert, A. K., Zarro, D. M., Snow, F., Thomsen, K., and Henneck, R. (2002). The Reuven Ramaty High-Energy Solar Spectroscopic Imager (RHESSI). *Solar Physics*, 210:3–32.
- Liu, W. and Ofman, L. (2014). Advances in Observing Various Coronal EUV Waves in the SDO Era and Their Seismological Applications (Invited Review). *Solar Physics*, 289(9):3233–3277.
- Mason, J. P. and Hoeksema, J. T. (2010). Testing Automated Solar Flare Forecasting With 13 Years of Michelson Doppler Imager Magnetograms. *The Astrophysical Journal*, 723:634–640.
- Mason, J. P., Woods, T. N., Caspi, A., Thompson, B. J., and Hock, R. A. (2014). MECHANISMS AND OBSERVATIONS OF CORONAL DIMMING FOR THE 2010 AUGUST 7 EVENT. *The Astrophysical Journal*, 789(1):61.
- Muhr, N., Veronig, A. M., Kienreich, I. W., and Temmer, M. (2011). Analysis of Characteristic Parameters of Large-Scale Coronal Waves Observed by the Solar-Terrestrial Relations Observatory/Extreme Ultraviolet Imager. *The Astrophysical Journal*, 89:89.
- National Research Council (2008). Severe Space Weather Events - Understanding Societal and Economic Impacts. page 131.
- Palo, S., Li, X., Gerhardt, D., Turner, D., Kohnert, R., Hoxie, V., and Batiste, S. (2010). Conducting Science with a CubeSat: The Colorado Student Space Weather Experiment.
- Parker, E. N. (1988). Nanoflares and the solar X-ray corona. *The Astrophysical Journal*, 330:474.
- Pearson, K. (1895). Note on Regression and Inheritance in the Case of Two Parents. *Proceedings of the Royal Society of London*, 58:240–242.
- Pesnell, W. D., Thompson, B. J., and Chamberlin, P. C. (2012). The Solar Dynamics Observatory (SDO). *Solar Physics*, 275:3–15.

- Peterson, J. and Fabian, A. (2006). X-ray spectroscopy of cooling clusters. *Physics Reports*, 427(1):1–39.
- Peterson, W. K., Stavros, E. N., Richards, P. G., Chamberlin, P. C., Woods, T. N., Bailey, S. M., and Solomon, S. C. (2009). Photoelectrons as a tool to evaluate spectral variations in solar EUV irradiance over solar cycle timescales. *Journal of Geophysical Research*, 114:A10304.
- Pohjolainen, S., Vilmer, N., Khan, J. I., and Hillaris, A. E. (2005). Early signatures of large-scale field line opening Multi-wavelength analysis of features connected with a halo CME event. *Astronomy & Astrophysics*, 434:329–341.
- Reinard, A. A. and Biesecker, D. A. (2008). Coronal Mass Ejection-Associated Coronal Dimmings. *The Astrophysical Journal*, 674:576–585.
- Reinard, A. A. and Biesecker, D. A. (2009). The Relationship Between Coronal Dimming and Coronal Mass Ejection Properties. *The Astrophysical Journal*, 705(1):914–919.
- Robbrecht, E. and Wang, Y.-M. (2010). The Temperature-Dependent Nature of Coronal Dimmings. *The Astrophysical Journal Letters*, 720:88–92.
- Rodgers, E. M., Bailey, S. M., Warren, H. P., Woods, T. N., and Eparvier, F. G. (2006). Soft X-ray irradiances during solar flares observed by TIMED-SEE. *Journal of Geophysical Research*, 111(A10):A10S13.
- Rompolt, . (1967). The H α Radiation Field in the Solar Corona for Moving Prominences. *Acta Astronomica*, 17.
- Schiller, Q., Gerhardt, D., Blum, L., Li, X., and Palo, S. (2014a). Design and scientific return of a miniaturized particle telescope onboard the Colorado Student Space Weather Experiment (CSSWE) CubeSat. In *2014 IEEE Aerospace Conference*, pages 1–14. IEEE.
- Schiller, Q., Li, X., Blum, L., Tu, W., Turner, D. L., and Blake, J. B. (2014b). A nonstorm time enhancement of relativistic electrons in the outer radiation belt. *Geophysical Research Letters*, 41(1):7–12.
- Schiller, Q. and Mahendrakumar, A. (2010). REPTile: A Miniaturized Detector for a CubeSat Mission to Measure Relativistic Particles in Near-Earth Space.
- Schlemm, C. E., Starr, R. D., Ho, G. C., Bechtold, K. E., Hamilton, S. A., Boldt, J. D., Boynton, W. V., Bradley, W., Fraeman, M. E., Gold, R. E., Goldsten, J. O., Hayes, J. R., Jaskulek, S. E., Rossano, E., Rumpf, R. A., Schaefer, E. D., Strohbehn, K., Shelton, R. G., Thompson, R. E., Trombka, J. I., and Williams, B. D. (2007). The X-Ray Spectrometer on the MESSENGER Spacecraft. *Space Science Reviews*, 131(1-4):393–415.
- Schrijver, C. J. and Higgins, P. A. (2015). A Statistical Study of Distant Consequences of Large Solar Energetic Events. *Solar Physics*, 290(10):2943–2950.
- Schrijver, C. J. and Title, A. M. (2011). Long-range magnetic couplings between solar flares and coronal mass ejections observed by SDO and STEREO. *Journal of Geophysical Research*, 116(A4):69–80.

- Solomon, S. C., Bailey, S. M., and Woods, T. N. (2001). Effect of solar soft X-rays on the lower ionosphere. *Geophysical Research Letters*, 28(11):2149–2152.
- Sterling, A. C. and Hudson, H. S. (1997). YOHKOH SXT OBSERVATIONS OF X-RAY DIMMING ASSOCIATED WITH A HALO CORONAL MASS EJECTION. *The Astrophysical Journal*, 491:L55–L58.
- Swings, P. (1941). Complex Structure of Cometary bands Tentatively Ascribed to the Contour of the Solar Spectrum. *Lick Observatory Bulletin*, 508.
- Thompson, B. J., Cliver, E. W., Nitta, N. V., Delannée, C., and Delaboudiniere, J. P. (2000). Coronal Dimmings and Energetic CMEs in April-May 1998. *Geophysical Research Letters*, 27(10):1431–1434.
- Tian, H., McIntosh, S. W., Xia, L., He, J., and Wang, X. (2012). What Can We Learn About Solar Coronal Mass Ejections, Coronal Dimmings, and Extreme-Ultraviolet Jets Through Spectroscopic Observations? *The Astrophysical Journal*, 748(2):106.
- Vourlidas, A., Howard, R. A., Esfandiari, E., Patsourakos, S., Yashiro, S., and Michalek, G. (2010). Comprehensive Analysis of Coronal Mass Ejection Mass and Energy Properties Over a Full Solar Cycle. *The Astrophysical Journal*, 722:1522–1538.
- Vourlidas, A., Howard, R. A., Esfandiari, E., Patsourakos, S., Yashiro, S., and Michalek, G. (2011). ERRATUM : COMPREHENSIVE ANALYSIS OF CORONAL MASS EJECTION MASS AND ENERGY PROPERTIES OVER A FULL SOLAR CYCLE (2010 , ApJ , 722 , 1522). 59:2010–2012.
- Vourlidas, A., Subramanian, P., Dere, K. P., and Howard, R. A. (2000). LargeAngle Spectrometric Coronagraph Measurements of the Energetics of Coronal Mass Ejections. *The Astrophysical Journal*, 534(1):456–467.
- Wang, Y. and Zhang, J. (2007). A Comparative Study between Eruptive XClass Flares Associated with Coronal Mass Ejections and Confined XClass Flares. *The Astrophysical Journal*, 665(2):1428–1438.
- Wang, Y. and Zhang, J. (2008). A Statistical Study of Solar Active Regions That Produce Extremely Fast Coronal Mass Ejections. *The Astrophysical Journal*, 680(2):1516–1522.
- Woods, T. N. and Chamberlin, P. C. (2009). Comparison of solar soft X-ray irradiance from broadband photometers to a high spectral resolution rocket observation. *Advances in Space Research*, 43:349–354.
- Woods, T. N., Chamberlin, P. C., Peterson, W. K., Meier, R. R., Richards, P. G., Strickland, D. J., Lu, G., Qian, L., Solomon, S. C., Iijima, B. A., Mannucci, A. J., and Tsurutani, B. T. (2008). XUV Photometer System (XPS): Improved Solar Irradiance Algorithm Using CHIANTI Spectral Models. *Solar Physics*, 250(2):235–267.
- Woods, T. N., Eparvier, F. G., Bailey, S. M., Chamberlin, P. C., Lean, J., Rottman, G. J., Solomon, S. C., Tobiska, W. K., and Woodraska, D. L. (2005a). Solar EUV Experiment (SEE): Mission overview and first results. *Journal of Geophysical Research*, 110:A01312.

- Woods, T. N., Eparvier, F. G., Hock, R. A., Jones, A. R., Woodraska, D. L., Judge, D., Didkovsky, L., Lean, J., Mariska, J. T., Warren, H., McMullin, D., Chamberlin, P. C., Berthiaume, G., Bailey, S. M., Fuller-Rowell, T., Sojka, J., Tobiska, W. K., and Viereck, R. (2012). Extreme Ultraviolet Variability Experiment (EVE) on the Solar Dynamics Observatory (SDO): Overview of Science Objectives, Instrument Design, Data Products, and Model Developments. *Solar Physics*, 275:115–143.
- Woods, T. N., Hock, R. A., Eparvier, F. G., Jones, A. R., Chamberlin, P. C., Klimchuk, J. A., Didkovsky, L., Judge, D., Mariska, J. T., Warren, H. P., Schrijver, C. J., Webb, D. F., Bailey, S. M., and Tobiska, W. K. (2011). New Solar Extreme-Ultraviolet irradiance Observations During Flares. *The Astrophysical Journal*, 739:59.
- Woods, T. N., Rottman, G., and Vest, R. (2005b). XUV Photometer System (XPS): Overview and Calibrations. *Solar Physics*, 230(1-2):345–374.
- Yashiro, S., Gopalswamy, N., Akiyama, S., Michalek, G., and Howard, R. A. (2005). Visibility of coronal mass ejections as a function of flare location and intensity. *Journal of Geophysical Research*, 110(A12):A12S05.
- Zharkova, V. V., Arzner, K., Benz, A. O., Browning, P., Dauphin, C., Emslie, A. G., Fletcher, L., Kontar, E. P., Mann, G., Onofri, M., Petrosian, V., Turkmani, R., Vilmer, N., and Vlahos, L. (2011). Recent Advances in Understanding Particle Acceleration Processes in Solar Flares. *Space Science Reviews*, 159(1-4):357–420.
- Zhukov, A. N. and Auchère, F. (2004). On the nature of EIT waves, EUV dimmings and their link to CMEs. *Astronomy & Astrophysics*, 427:705–716.